(23–27). tRNase ZL functions in the same way as the 4 nt-recognizing RNA cutter RNase 65, by forming a complex with a 3′-truncated tRNA (23). Partial HIV-1 RNA targets can be cleaved site specifically by the enzyme, once the targets form pre-tRNA-like structures with the aid of appropriate 5′-half-tRNAs (24). RNA heptamers that form acceptor-stem-like duplexes with their targets through base pairing can also direct the specific cleavage of target RNAs by tRNase ZL *in vitro* with the same efficiency as the original 5′-half-tRNAs (25,26). However, in this case, the target sites are restricted to regions immediately downstream of stable hairpin structures resembling the T stem/loop. Together with such flexibility in substrate recognition, the ubiquity and constitutive expression of tRNase ZL suggests that this enzyme can be utilized for specific cleavage of cellular RNAs by introducing the appropriate sgRNAs into living cells (27).

Recently, we demonstrated the efficacy of this method in specifically targeting RNA in living cells by introducing sgRNAs encoded either by expression plasmids or by 2′-*O*-methyl RNAs (28). The expression of the exogenous reporter genes for *Escherichia coli* chloramphenicol acetyltransferase and firefly luciferase were downregulated for at least 48 h by appropriately designed sgRNAs in cultured human and dog cells. A 2′-*O*-methyl heptamer designed to target the endogenous Bcl-2 mRNA was also successful in Sarcoma 180 cells.

In the present study, we investigated whether the sgRNA/tRNase ZL strategy could also be an effective approach to gene therapy for AIDS. Several sgRNAs targeted against HIV-1 mRNA, and expressed by plasmid and retroviral vectors, were tested for their ability to repress its expression. Our findings confirmed that they were effective in both COS and Jurkat cells.

MATERIALS AND METHODS

Plasmid construction and retroviral vector production

Expression cassettes for the sgRNA were constructed under the control of the human methionine tRNA promoter. The expressed sgRNA was targeted against either the packaging signal or the *gag* portion of the HIV-1_{NL4-3} strain (Figure 1B). Enhanced green fluorescent protein (EGFP) is a red-shifted variant of wild-type GFP (29,30), which has been optimized for brighter fluorescence and higher expression in mammalian cells (excitation maximum = 488 nm; emission maximum = 507 nm). A DNA fragment containing EGFP was excised from the plasmid pLEGFP (Promega, Madison, WI) by digestion with BamHI–NaeI. The EGFP fragment was ligated to the EcoRI and XhoI sites of pSV2neo/sgR to generate pSV2neo/sgRG. The Moloney strain of the murine leukaemia virus (MoMLV)-based sgRNA pLsgRGSN (Figure 1B) was constructed by inserting the EcoRI and XhoI fragments from plasmid pSV2neo/sgRG, along with sgRNAs and EGFP genes, into the EcoRI and XhoI sites of the retroviral vector pLXSN (31).

Vesicular stomatitis virus glycoprotein-pseudotyped retrovirus vector supernatants were generated by transient transfection of 293T cells, as described previously (32), using 20 μg of vector plasmid, 10 μg of pMLVΔψΔenv (33) and 10 μg of pVSVG envelope plasmid (32,34). Thereafter, supernatants were collected every 12 h for 3 days, filtered through a 0.45 μm pore-size filter (Nalgene, Rochester, NY) and concentrated 100- to 1000-fold by ultracentrifugation (35,36). Pellets were resuspended in serum-free DMEM and stored at −80°C until they were used.

Transduction of target cells

A total of 3×10^5 Jurkat cells per well were plated out in 6-well plates 1 day before transduction. After 24 h, virus supernatant was added together with polybrene (final concentration = 5–8 μg/ml) and the cells were incubated at 25°C overnight. The medium was then replaced with fresh medium containing G418 (500 μg/ml; GIBCO-BRL, Rockville, MD). After 10 days, cell pools that were resistant to G418 were established.

Cells and transfection

COS and Jurkat cells were grown in RPMI 1640 medium (Sigma, St. Louis, MO) supplemented with 10% (v/v) heat-inactivated fetal bovine serum (FBS) at 37°C in a 5% CO_2 atmosphere. Transfection was carried out using the FuGENE^{TM}6 reagent (Roche Diagnostics, Tokyo, Japan) according to the manufacturer's protocol.

Luciferase assay

Luciferase activity was measured with the PicaGene kit (Toyo-inki, Tokyo, Japan) according to the manufacturer's protocol. The envelope-defective HIV-1 NL_{4-3}-based retroviral vector containing a luciferase-expression marker (pNL_{4-3}-luc) (32) was generated as follows. The *nef* gene sequences of the HIV-1 NL_{4-3} genome were substituted with the firefly luciferase gene, and the envelope gene sequences located between two Bgl II restriction endonuclease sites were deleted (Figure 1B). The transfection reagent, FuGENE^{TM}6, was used to transfect COS cells with the plasmids expressing sgRNA and pNL_{4-3}-luc. The COS cells were lysed using 200 μl of PicaGene cell lysis buffers (Toyo-inki) for 15 min and detached from the plate by scraping. Cellular debris were then removed by centrifugation. The luminescent signal was quantitated by adding 10 μl clarified lysate to 100 μl luminous substrate, and the level of fluorescence was recorded immediately using a luminometer (Lumat LB 9507; Berthold, Bad Wildbad, Germany).

The amount of firefly luciferase activity was normalized with reference to the protein concentration in the lysate. The protein was quantitated using the BCA Protein Assay Reagent kit (Pierce, IL), which is based on bicinchoninic acid.

Localization of sgRNA

The cytoplasmic fraction was prepared from collected cells after washing twice with phosphate-buffered saline (PBS). The cells were resuspended in digitonin lysis buffer (50 mM HEPES-KOH, pH 7.5, 50 mM potassium acetate, 8 mM $MgCl_2$, 2 mM EGTA and 50 μg/ml digitonin) and incubated on ice for 10 min. The lysate was centrifuged at 1000 *g* for 5 min and the resultant supernatant was collected and used as the cytoplasmic fraction. The pellets were resuspended in NP-40 lysis buffer (20 mM Tris–HCl, pH 7.5, 50 mM KCl, 10 mM NaCl, 1 mM EDTA and 0.5% NP-40) and incubated on ice for 10 min. The resultant lysate was used as the nuclear fraction. Cytoplasmic and nuclear RNA were extracted and purified

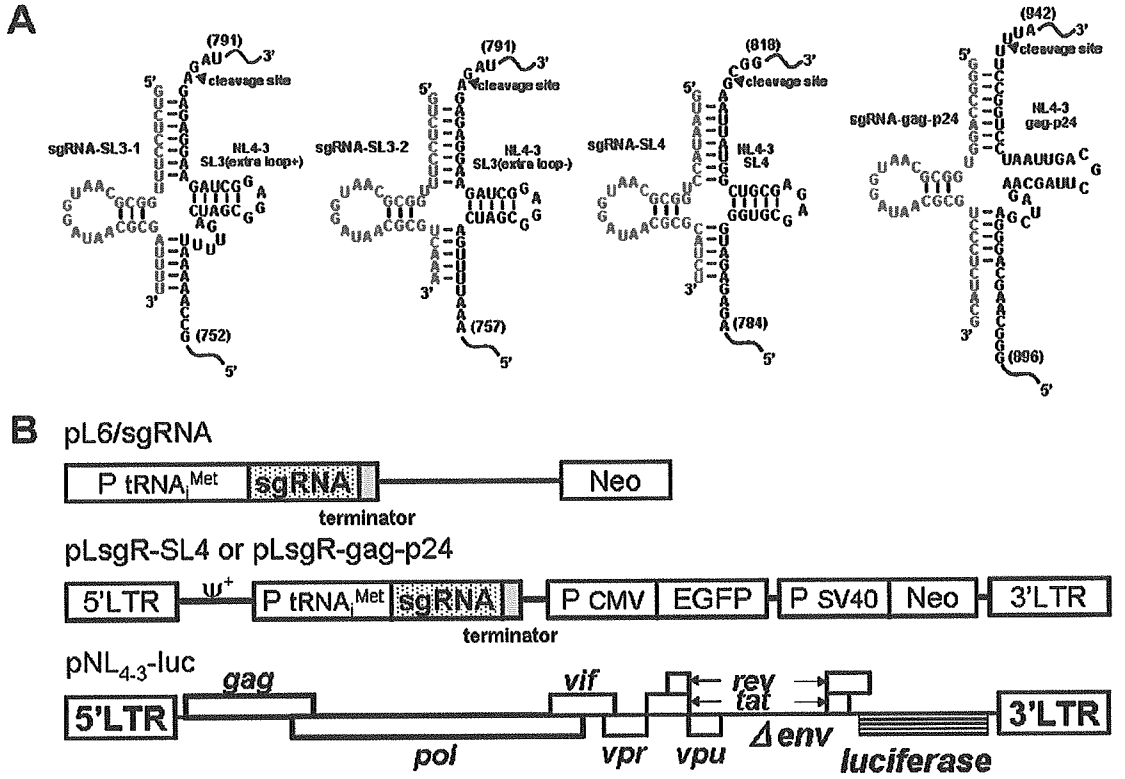

Figure 1. (A) Plausible secondary structures of complexes of the three target sites within the HIV-1 genome [the ψ site (SL3-stem loop), the SL4-stem-loop site and gag-24 within the HIV-1 gene] with the modified 5′-half-tRNA^{Arg} (sgRNA-SL3-1, 2, SL-4 and gag-p24) containing 7 and 5 nt sequences complementary to the target HIV-1 ψ site and the *gag* gene. The arrow indicates the tRNase Z cleavage point. (**B**) Schematic diagrams of the sgRNA-expression plasmids, the retroviral vector and the HIV-1 luciferase reporter-vector constructs. Methods for the construction of the sgRNA-expression plasmids (pL6-sgRNA-SL3-1, pL6-sgRNA-SL3-2, pL6-sgRNA-SL4 and pL6-sgRNA-gag-p24) and the retroviral vectors (pLsgRGSN-SL4 and pLsgRGSN-gag-p24) are detailed in Materials and Methods. The envelope-defective HIV-1 NL$_{4-3}$-based retroviral vector contained a luciferase-expression marker (pNL$_{4-3}$-luc). This HIV-1-based vector was generated by substituting the *nef* gene sequences of the HIV-1$_{NL4-3}$ genome with the firefly luciferase gene, and deleting the envelope gene sequences located between two Bgl II restriction endonuclease sites (32).

from their respective fractions using ISOGEN reagent (Wako, Osaka, Japan). RNA samples were treated with DNase I (Takara Shuzo, Shiga, Japan) according to the manufacturer's instructions. RT–PCR assays were performed using an RT–PCR High-Plus kit (Toyobo, Osaka, Japan) according to the manufacturer's protocol. The nucleotide sequences of the sgRNA-SL4 primers were 5′-TACTGTGAGACCGTGTGCTT-3′ (F-primer) and 5′-TACTGTGAGACCGTGTGCTT-3′ (R-primer). The nucleotide sequences of the U6 primers were 5′-CAGACATGATAAGATACATTGATGAGTTTG-3′ (F-primer) and 5′-CGGGATCCCGGCAATAGCATCACAAATTTC-3′ (R-primer).

Cleavage activities of sgRNA in COS cells

COS cells were grown to ~80% confluence (3×10^5 cells) and transfected with 3 μg each of the sgRNA vector and the pNL$_{4-3}$-luc plasmid. The cells were incubated for 2 days before total cellular RNA was isolated. RNA samples were treated with DNase I according to the manufacturer's specifications, and RT–PCR assays were carried out as described above. The levels of cleaved and uncleaved HIV-1 mRNAs were quantified by RT–PCR with an endogenous internal standard, GAPDH. A sample of 1 μg of total RNA was used as the template with the SL3, SL4, p24 and GAPDH primers (20 pmol each). Reverse transcription in a final reaction volume of 50 μl was carried out at 60°C for 30 min. The cDNA products were then amplified by PCR using amplification conditions comprising 40 cycles of 94°C for 60 s and 60°C for 90 s. The SL3-F1 (5′-TTGCTGAAGCGCGCACGGCA-3′) and p24-F1 (5′-TAAGGCCAGGGGGAAAGAAACAATATAAAC-3′) primer pair, and the SL3-R and SL4-R (5′-GTTCTTCTGATCCTGTCTGAAGGGATGGTT-3′) and p24-R (5′-GCCCCTGGAGGTTCTGCACTATAGGGTAAT-3′) primer pair, only generated a cDNA product from the uncleaved HIV-1 mRNA (RT–PCR products I and III, SL3 = 310 bp; RT–PCR product V, gag-p24 = 360 bp). The SL3-F2 (5′-TAAATGGGAAAAAATTCGGT-3′), SL4-F2 (5′-ATTCGGTTAAGGCCAGGGGG-3′) and p24-F2 (5′-AGACAAATACTGGGACAGCTACAACCATCC-3′) primer pairs were used to generate cDNA products corresponding to the cleaved and uncleaved sgRNA sequences, respectively, thereby identifying both sets of products. The SL3, SL4 and p24 yielded the RT–PCR products II (SL3 = 182 bp), IV (SL4 = 168 bp) and VI (p24 = 250 bp), whereas the GAPDH-F and R-primers amplified a fragment of the GAPDH gene (0.45 kb) as an internal control.

In vitro RNA synthesis

The partial HIV-1 RNA targets (T-SL3-1 and T-gag-p24) and the sgRNAs (sgRNA-SL3-1 and sgRNA-gag-p24) were synthesized from the corresponding synthetic DNA templates with an additional unencoded 'G' at the 5′ end corresponding to the −1 in a tRNA to enhance its transcriptional efficiency, using T7 RNA polymerase (Takara Shuzo). The sequences of the target RNAs and sgRNAs were as follows: 5′-GCCAAA-AAUUUUGACUAGCGGAGGCUAGAAGGAGAGAGAU-GGGUGC-3′ (T-SL3-1); 5′-GCAAGCAGGGAGCUAGAA-CGAUUCGCAGUUAAUCCUGGCCUUUUAGAGACA-3′ (T-gag-p24); 5′-GUCUCCUUUGGCGCAAUGGAUAACG-CGAUUUU-3′ (sgRNA-SL3-1); and 5′-GGGCCAGGU-GGCGCAAUGGAUAACGCGUCCCUCUACG-3′ (sgRNA-gag-p24). The transcription reactions were carried out under the conditions recommended by the manufacturer (Takara Shuzo), and after synthesis the RNAs were purified by denaturing gel electrophoresis. The RNA transcripts for T-SL3-1 and T-gag-p24 were subsequently labelled with fluorescein (F) according to the manufacturer's protocol (Amersham Pharmacia Biotech, NJ). Briefly, after the removal of the 5′-phosphates of the transcribed RNAs using bacterial alkaline phosphatase (Takara Shuzo), the RNAs were phosphorylated with T4 polynucleotide kinase (Takara Shuzo) and ATPγS. Then, a single fluorescein moiety was appended to the 5′-phosphorothioate site. The resulting fluorescein-labelled RNAs were gel-purified before being used in the assays.

In vitro RNA-cleavage assays

The *in vitro* RNA-cleavage assays for the fluorescein-labelled target RNA, T-SL3-1 or T-gag-p24 (0.1 pmol), were performed with pig liver tRNase ZL (20 ng) in the presence of unlabelled sgRNA-SL3-1 or sgRNA-gag-p24 (5 or 10 pmol) in a mixture (6 µl) containing 10 mM Tris–HCl (pH 7.5), 1.5 mM DTT and 10 mM $MgCl_2$ at 50°C for 10 min. After resolution of the reaction products by electrophoresis through a 10% polyacrylamide/8 M urea sequencing gel, the gel was analysed using a Typhoon 9210 (Amersham Pharmacia Biotech).

HIV-1-challenge assay

G418-resitant cell pools were incubated for 4 h with HIV-1_{NL4-3} at a multiplicity of infection of 0.01. After two washes with PBS, the cells were cultured in RPMI 1640 medium (Sigma) supplemented with 10% (v/v) heat-inactivated FBS. The supernatant was collected on days 1, 3, 6, 9, 12, 15 and 18 after viral infection, and the culture medium was assayed for HIV-1 gag-p24 antigen using CLEIA (Lumipulse, Fujirebio, Tokyo, Japan) according to the manufacturer's protocol (37).

RESULTS AND DISCUSSION

sgRNAs can inhibit HIV-1 gene expression

We demonstrated in a previous study that antisense phosphorothioate oligonucleotides (S-ODNs) complementary to the *gag* mRNA (SL4-stem loop), containing the HIV-1 *gag* AUG initiation codon, have potent anti-HIV activity in infected cultured cells. This activity was strong compared with oligonucleotides targeted to the splice acceptor of the *tat* gene and the AUG initiation codon of the *rev* gene (38). We have also shown *in vitro* that mammalian tRNase ZL with the aid of a 5′-half-tRNA-like sgRNA can cleave a partial HIV-1 mRNA substrate containing the p24 site of the HIV-1 *gag* gene (24). Therefore, it would be reasonable to select the gag AUG site (designated SL4) and the gag-p24 site to examine the efficacy of the sgRNA method in cultured cells. The HIV-1 packaging signal (ψ) that efficiently targets genomic RNA into nascent virions (39,40) and the ψ site (designated SL3) was chosen as an additional target site for tRNase ZL.

The 5′-half-tRNA-type sgRNAs, designated sgRNA-SL3-1 and sgRNA-SL3-2 (extra loop-), were designed to form

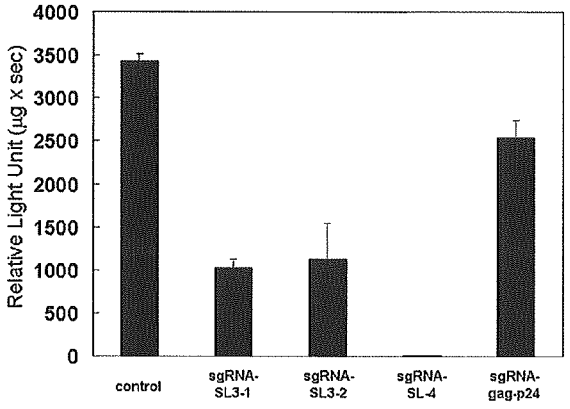

Figure 2. Luciferase activity of the pNL_{4-3}-luciferase (pNL_{4-3}-luc) fusion gene in COS cells. The cells were co-transfected with the target-expressing plasmid pNL_{4-3}-luc and either the pL6 plasmid encoding the sgRNAs or pL6-ter serving as a negative control for inhibition using the FuGENE™6 transfection reagent. The plotted data were averaged from three independent experiments, and the bars represent ±SD.

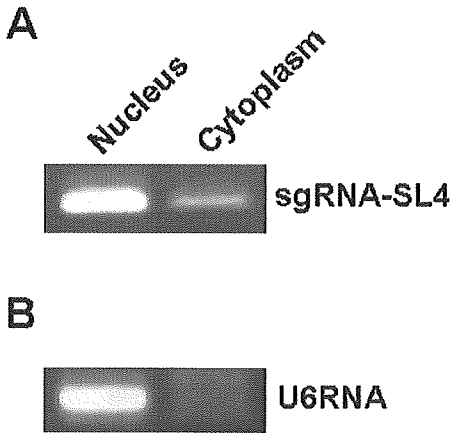

Figure 3. Intracellular localization of the $tRNA_i^{met}$–sgRNA. To analyse the degree of intracellular localization of $tRNA_i^{met}$–sgRNA, nuclear and cytoplasmic fractions were prepared from transformants that expressed sgRNA-SL4 and the total RNA was extracted from each. The transcribed sgRNA-SL4 was detected using RT–PCR analysis with a primer specific for the sgRNA. (**A**) RT–PCR analyses revealed that $tRNA_i^{met}$–sgRNA-SL4 was located almost exclusively in the nucleus, as predicted. (**B**) Nuclear and cytoplasmic fractions were examined with a probe specific for the transcript of the U6 gene (control).

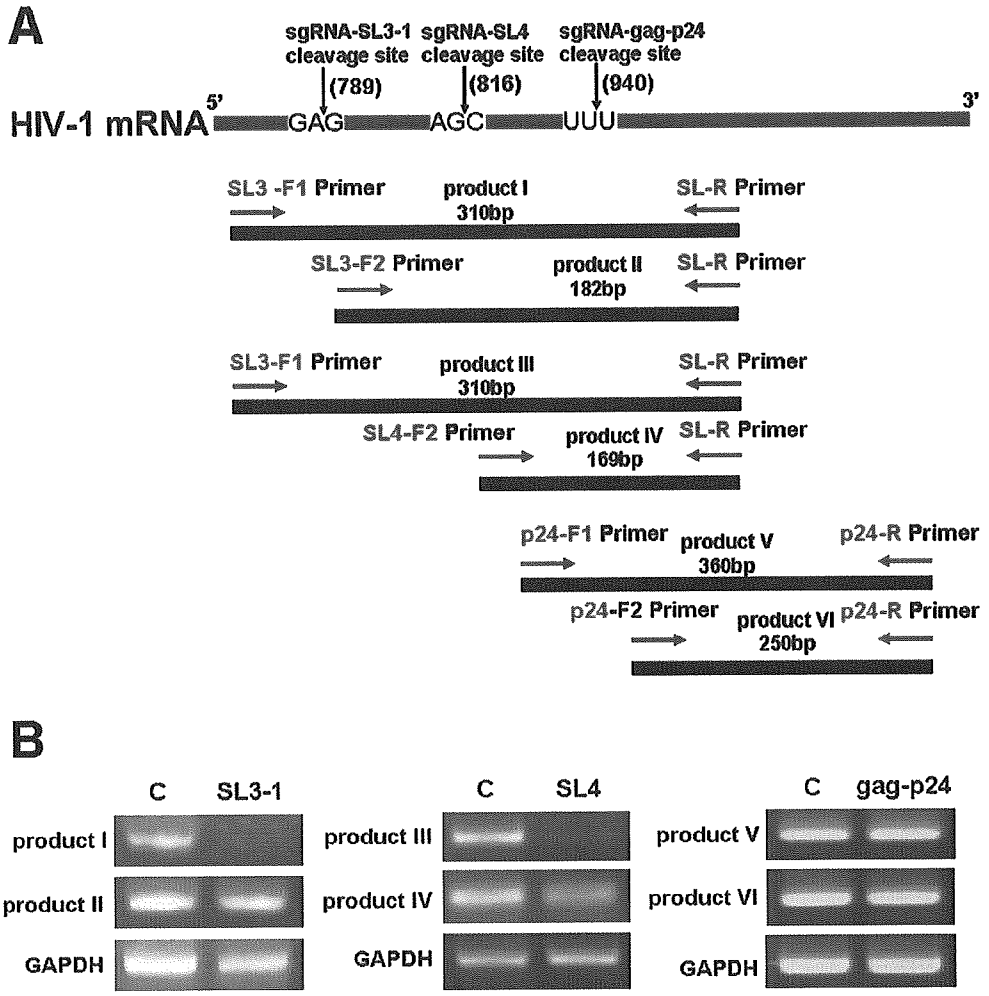

Figure 4. RT–PCR analyses of HIV-1 mRNA expression. RT–PCR analyses of uncleaved (product I), and total cleaved and uncleaved (product II), HIV-1 mRNA were performed using HIV-1 *gag*-specific primers with concurrent amplification of GAPDH mRNA. (**A**) Schematic representation of HIV-1-specific primer sites with respect to HIV-1 mRNA: F1 primers, SL3 and p24; F2 primers, SL3, SL4 and p24; R-primers, SL3, SL4 and p24. (**B**) RT–PCR amplification products analysed by 2% agarose gel electrophoresis with ethidium bromide staining.

pre-tRNA-like complexes with SL3. They contained or lacked an extra loop, respectively (Figure 1A). sgRNA-SL4 without an extra loop was intended to make a pre-tRNA-like complex with SL4, and sgRNA-gag-p24 with an extra loop was designed to form a pre-tRNA-like complex with the gag-p24 site (Figure 1A).

The sgRNA-expression plasmids were constructed in the mammalian expression plasmid pL6 (41,42) and (Figure 1B) by inserting synthetic DNA sequences between the human $tRNA_i^{met}$ promoter sequence and the RNA polymerase III termination-signal sequence. RT–PCR analysis was used to examine the expression of the sgRNA by these plasmids in transfected COS cells. A high level of sgRNA was expressed in the transfected cells, driven by a $tRNA_i^{met}$ promoter (data not shown).

A transient-expression assay was used to test the ability of pL6-expressed sgRNA-SL3-1 and 2, sgRNA-SL4 and sgRNA-gag-p24 to inhibit HIV-1 expression. COS cells were co-transfected with the sgRNA plasmids and an HIV-1_{NL4-3}-based vector containing a luciferase-expression maker (pNL_{4-3}-luc) (31), then suppression of HIV-1 was assessed in a single-cycle infectivity assay (Figure 2). HIV-1_{NL4-3}-based luciferase activity was recorded using the control plasmid vector L6-ter with only the $tRNA_i^{met}$ promoter and terminator sequences, rather than the sgRNA-expression plasmid. Both sgRNA-SL3-1 and sgRNA-SL3-2 showed good inhibition of HIV-1 expression in the cultured cells, suggesting that the extra loop in the pre-tRNA-like complex is not important for tRNase ZL recognition (Figure 2). Amazingly, HIV-1 gene expression was almost completely inhibited by sgRNA-SL4, but only moderately suppressed by sgRNA-gag-p24. This might be because endogenous tRNase ZL has difficulty in recognizing the sgRNA-gag-p24/target complex, possibly due to the lack of a stable 'T-stem-loop' structure in the target, as indicated by the *in vitro* cleavage assays described below. These results imply that the sgRNA/tRNase

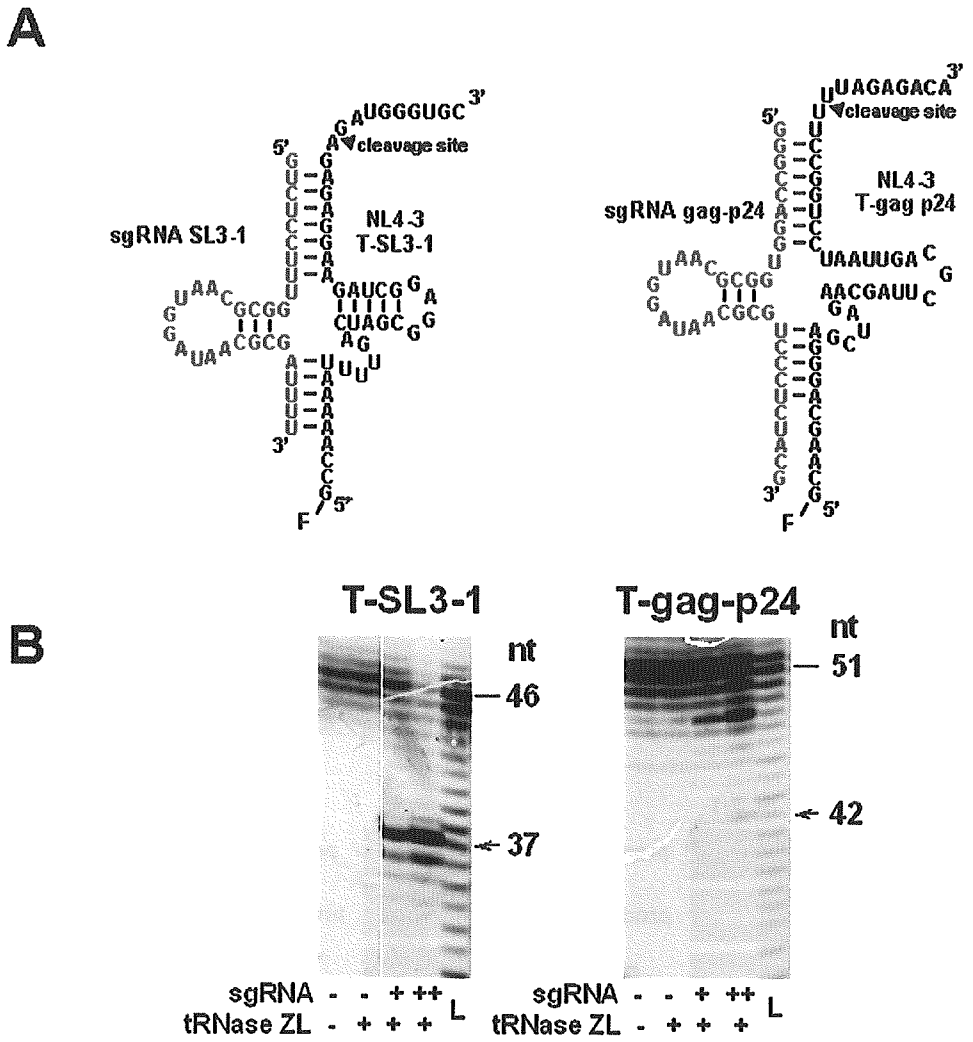

Figure 5. sgRNA guided specific HIV-1 mRNA cleavage by *in vitro* tRNase ZL assays. (**A**) Secondary structures of the substrate-HIV-1 SL3-1 (extra loop) and gag-24 complexes with sgRNA-SL3-1 and sgRNA-gag-p24. (**B**) The assays for the fluorescein (F)-labelled target RNA T-SL3-1 or T-gag-p24 (0.1 pmol) were performed with pig liver tRNase ZL (20 ng) in the presence of the unlabelled sgRNA-SL3-1 or sgRNA-gag-p24 (5 or 10 pmol) at 50°C for 10 min. The cleavage reactions were analysed using a 10% polyacrylamide/8 M urea sequencing gel. The target RNA and the primary 5′-cleavage product are indicated by a bar and arrow, respectively, together with their size in nucleotides. L denotes the alkaline ladder of each fluorescein-labelled target RNA.

ZL strategy is effective in reducing the level of the HIV-1 gene expression, although the efficiency of inhibition differs according to the sgRNAs used.

Intracellular localization of the $tRNA_i^{met}$–sgRNA

Co-localization of sgRNAs, their RNA targets and tRNase ZL is important for efficient downregulation; therefore, we examined the intracellular location of sgRNA-SL4 (41,42). Transformed cells expressing sgRNA-SL4 were separated into nuclear and cytoplasmic fractions, and the total RNA was extracted from each. sgRNA-SL4 was detected using RT–PCR analysis with a primer specific for the sgRNA. This revealed that they were located almost exclusively in the nucleus (80%) (Figure 3).

The inhibitory effect of sgRNA occurs through target RNA degradation by tRNase ZL

The contribution of HIV-1 mRNA cleavage to the sgRNA-mediated anti-HIV-1 effect was examined by measuring HIV-1 mRNA levels (43,44). Two sets of RT–PCR reactions were used to establish the level of HIV-1 mRNA uncleaved at the target site by tRNase ZL [products I (310 bp), III (310 bp) and V (360 bp)], and the total amount of HIV-1 mRNA at the target site [products II (182 bp), IV (169 bp) and VI (250 bp)], i.e. both cleaved and uncleaved. The uncleaved HIV-1 mRNA was amplified by primers SL3-F1 and gag-p24-F1, and the SL3-R, SL4-R and gag-p24-R primers (Figure 4A). The levels of products I, III and V were expected to decrease after cleavage of the HIV-1 mRNA. The levels of products II, IV and VI reflected the total amount of HIV-1 mRNA (cleaved and

uncleaved SL3, SL4 and gag-p24), as the 3′ fragment of cleaved HIV-1 mRNA remained a viable template for amplification in this PCR. The results, which are shown in Figure 4B, indicate that the sgRNA-SL3-1- and SL4-dependent expression system reduced the amount of HIV-1 mRNA [products I (92%) and IV (97%)], whereas transfection with pNL_{4-3}-luc/sgRNA-gag-p24 did not significantly alter uncleaved HIV-1 mRNA expression in COS cells (Figure 4B). These data are consistent with the results of the luciferase assays and suggest that the inhibitory effect of sgRNA is achieved through target RNA degradation by tRNase ZL.

sgRNA-gag-p24 barely directs *in vitro* HIV-1 RNA cleavage by tRNase ZL

sgRNA-gag-p24 was much less effective than the other sgRNAs in suppressing HIV-1 gene expression in cells. We examined the reason for this by assessing its ability to guide HIV-1 RNA cleavage by tRNase ZL *in vitro*. The partial HIV-1 RNAs T-SL3-1 and T-gag-p24 containing SL3 and the gag p24 site, respectively, were synthesized *in vitro* with T7 RNA polymerase and 5′ end-labelled with fluorescein. sgRNA-SL3-1 and sgRNA-gag-p24 were also transcribed by T7 RNA polymerase *in vitro*. The ability of each sgRNA to induce cleavage of the corresponding target RNA by tRNase ZL was tested *in vitro*. The target T-SL3-1 was cleaved efficiently under the direction of sgRNA-SL3-1, whereas cleavage of the target T-gag-p24 by sgRNA-gag-p24 was highly inefficient (Figure 5), this was in agreement with the *in vivo* observations. Cleavage of each target occurred primarily 1 nt downstream of the nucleotide corresponding to the discriminator (Figure 5). These results indicate that sgRNA bound to its target HIV-1 mRNA, and cleavage of the pre-tRNA complexes with tRNase ZL occurred. It was therefore important to determine the localization of both the sgRNA and its target HIV-1 in the cells. The reduction in functional HIV-1 mRNA was consistent with tRNase ZL cleavage occurring at the post-transcriptional level.

Inhibition of HIV-1 gene expression by retroviral vector-mediated sgRNAs in human T cells

The inhibitory effect of HIV-1 expression by tRNase ZL-mediated sgRNAs was investigated in human T cells by constructing a MoMLV-based sgRNA retroviral vector. Most retroviral vectors used in experimental and clinical gene therapy are derived from the MoMLV (45). Retroviruses integrate into the chromosomal DNA, so their genome is stable in the host cells and is inherited by their progeny. Accordingly, long-term expression of a transduced gene can be achieved through retrovirus-mediated gene transfer. Other advantages of this vector include its broad host range and the availability of packaging cell lines for the large-scale production of high-titre vectors. It has previously been shown that an amphotropic MoMLV-based retrovirus vector can transduce a human T-cell line (46). We therefore expressed the sgRNA under the control of the promoter of a human $tRNA_i^{met}$ gene via a retroviral vector (Figure 1B). The plasmid pLsgRGSN (Figure 1B) was constructed by inserting the following elements into the EcoRI and XhoI sites of the retroviral vector pLXSN: an EcoRI and XhoI fragment from the plasmid pSV2neo/sgRG, sgRNAs and EGFP genes. We then obtained transduced Jurkat T cells

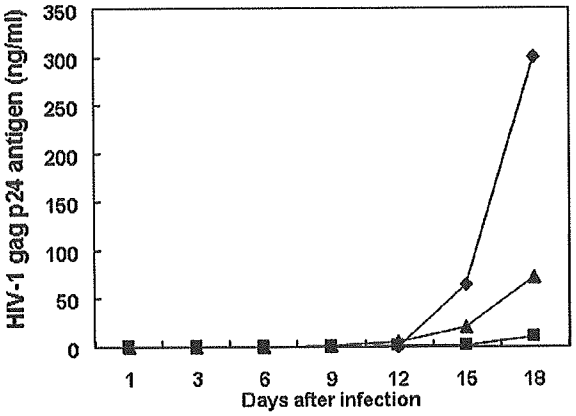

Figure 6. Inhibition of HIV-1 gag-p24 product in Jurkat cells expressing stably retrovirus vector-mediated sgRNA. Cells were cultured for 18 days after infection with $HIV\text{-}1_{NL4\text{-}3}$. Small aliquots of supernatant were prepared from each culture on days 1, 3, 6, 9, 12, 15 and 18. HIV-1 gag p24 antigen was determined using CLEIA (Lumipulse) according to the manufacturer's protocol (37): closed diamonds, pLGSN-Δ*sgR*; closed squares, pLsgRGSN-SL4; and closed triangles, pLsgRGSN-gag-p24.

stably expressing the sgRNAs. These Jurkat T cells were infected with wild-type $HIV\text{-}1_{NL4\text{-}3}$, and HIV-1gag-p24 antigen levels in the cell-free supernatant were measured at weekly intervals over 18 days. By day 18, the HIV-1 gag-p24 product was suppressed almost completely (~97%) in the cell cultures expressing sgRNA-SL4 (Figure 6). In contrast, sgRNA-gag-p24 and sgRNA-SL4 failed to inhibit viral expression under these experimental conditions. The difference between the effects of sgRNA-SL4 and sgRNA-gag-p24 in the HIV-1-challenged assay was due to the lack of base pairing in the hairpin structure resembling the T-stem-loop region.

In conclusion, we demonstrated the inhibition of HIV-1 gene products in cultured cells by inducing HIV-1 mRNA cleavage using a modified 5′-half-$tRNA^{Arg}$ (sgRNA) and mammalian tRNase ZL. The sgRNA/target HIV-1RNA complex formed a pre-tRNA-like structure with 5′-half-tRNA and a stable hairpin (3′-half-tRNA) structure resembling the T-stem-loop region. The $tRNA_i^{met}$–sgRNA transcript was expressed at high levels and localized in the nucleus. The greatest inhibitory effect on HIV-1 expression was achieved using sgRNA-SL4 targeting the HIV-1 *gag* gene. These results suggest that both sgRNA and its target HIV-1 mRNA were located in the nucleus, allowing specific cleavage by tRNase ZL. Furthermore, MoMLV-based sgRNA-SL4 could suppress sgRNA-dependent HIV-1 expression in human T cells. We believe that the use of mammalian tRNase ZL in conjunction with guide sequences represents a promising tool for the inactivation of genes in mammalian cells. Furthermore, the inhibition of HIV-1 using this approach demonstrates its potential as a therapeutic agent for AIDS.

ACKNOWLEDGEMENTS

We thank Prof. Y. Koyanagi for providing some of the plasmids, and Dr H. Takeuchi for technical assistance. This work was supported by a Grant-in-Aid for High Technology

Research (HTR) from the Ministry of Education, Science, Sports and Culture, Japan, by research grants from the Human Science Foundation (HIV-K-14719) and the Science Research Promotion Fund, and by an Academic Frontier Research Project Grant from the Promotion and Mutual Aid Corporation for the Private Schools of Japan. Y.H. is a Research Fellow of the HTR. Funding to pay the Open Access publication charges for this article was provided by HTR.

REFERENCES

1. Kelin,A.S., Klebba,C. and Hoelzer,D. (2000) Gene therapy of HIV-1 infection. In Unger,R.E., Kreuter,J. and Rubsaman-Waigmann,H. (eds.), *Antivirals Agent AIDS*. Marcel Dekker Inc., NY, 219–248.
2. Rigden,J.R., Ely,J.A., Macpherson,J.L., Gerlach,W.L., Sun,L.-Q. and Symonds,G.P. (1999) The use of ribozyme gene therapy for the inhibition of HIV replication and its pathogenic sequelae. In Rossi,J.J. and Couture,L.A. (eds.), *Intracellular Ribozyme Applications, Principles and Protocols*. Horizon Scientific Press, England, 93–102.
3. Dornburg,R. and Pomerantz,R.Z. (2000) Gene therapy and HIV-1 infection. In Templeton,N.S. and Lasic,D.D. (eds.), *Gene Therapy, Therapeutic Mechanisms and Strategies*. Marcel Dekker Inc., NY, 519–534.
4. Kurreck,J. (2003) Antisense technologies, improvement through novel chemical modifications. *Eur. J. Biochem.*, **270**, 1628–1644.
5. Jen,K.-Y and Gewirtz,A.M. (2000) Suppression gene expression by targeted disruption of messenger RNA available options and current strategies. *Stem Cells*, **18**, 307–319.
6. Bunnell,B.A. and Morgan,R.H. (1998) Gene therapy for infectious diseases. *Clin. Microbiol. Rev.*, **11**, 42–56.
7. Martinez,M.A., Clotet,B. and Este,J. (2002) RNA interference of HIV replication. *Trends Immunol.*, **23**, 559–561.
8. Lori,F., Guallini,P., Gulluzzi,L. and Lisziewicz,J. (2002) Gene therapy approaches to HIV infections. *Am. J. Pharmacogenomics*, **2**, 245–252.
9. Stevenson,M. (2003) Dissecting HIV-1 through RNA interference. *Nature Rev. Immunol.*, **3**, 851–858.
10. Scherer,L.J. and Rossi,J.J. (2003) Approaches for the sequence-specific knockdown of mRNA. *Nat. Biotechnol.*, **21**, 1457–1465.
11. Takaku,H. (2004) Gene silencing of HIV-1 by RNA interference. *Antivir. Chem. Chemother.*, **15**, 57–65.
12. Yuan,Y., Hwang,E.S. and Altman,S. (1992) Targeted cleavage of mRNA by human RNase P. *Proc. Natl Acad. Sci. USA*, **89**, 8006–8010.
13. Yuan,Y. and Altman,S. (1994) Selection of guide sequences that direct efficient cleavage of mRNA by human ribonuclease. *Science*, **263**, 1269–1273.
14. Guerrier-Takada,C., Li,Y. and Altman,S. (1995) Artificial regulation of gene expression in *Escherichia coli* by RNase P. *Proc. Natl Acad. Sci. USA*, **92**, 11115–11119.
15. Hnatyszyn,H., Spruillm,G., Youngm,A., Seivrightm,R. and Kraus,G. (2001) Long-term RNase P-mediated inhibition of HIV-1 replication and pathogenesis. *Gene Ther.*, **24**, 1863–1871.
16. Kraus,G., Geffin,R., Spruill,G., Young,A.K., Seivright,R., Cardona,D., Burzawa,J. and Hnatyszyn,H.J. (2002) Cross-clade inhibition of HIV-1 replication and cytopathology by using RNase P-associated external guide sequences. *Proc. Natl Acad. Sci. USA*, **99**, 3406–3411.
17. Barnor,J.S., Endo,Y., Habu,Y., Miyano-Kurosaki,N., Kitano,M., Yamamoto,H. and Takaku,H. (2004) Effective inhibition of HIV-1 replication in cultured cells by external guide sequences and ribonuclease P. *Bioorg. Med. Chem. Lett.*, **14**, 4941–4944.
18. Nashimoto,M. (1997) Distribution of both lengths and 5′ terminal nucleotides of mammalian pre-tRNA 3′ trailers reflects properties of 3′ processing endoribonuclease. *Nucleic Acids Res.*, **25**, 1148–1154.
19. Takaku,H., Minagawa,A., Takagi,M. and Nashimoto,M. (2003) A candidate prostate cancer susceptibility gene encodes tRNA 3′ processing endoribonuclease. *Nucleic Acids Res.*, **31**, 2272–2278.
20. Takaku,H., Minagawa,A., Takagi,M. and Nashimoto,M. (2004) The N-terminal half domain of the long form of tRNase Z is required for the RNase 65 activity. *Nucleic Acids Res.*, **32**, 4429–4438.
21. Tavtigian,S.V., Simard,J., Teng,D.H., Abtin,V., Baumgard,M., Beck,A., Camp,N.J., Carillo,A.R., Chen,Y., Dayananth,P. *et al.* (2001) A candidate prostate cancer susceptibility gene at chromosome 17p. *Nature Genet.*, **27**, 172–180.
22. Minagawa,A., Takaku,H., Takagi,M. and Nashimoto,M. (2004) The missense mutations in the candidate prostate cancer gene *ELAC2* do not alter enzymatic properties of its product. *Cancer Lett.*, in press.
23. Nashimoto,M. (1995) Conversion of mammalian tRNA 3′ processing endoribonuclease to four-base-recognizing RNA cutters. *Nucleic Acids Res.*, **23**, 3642–3647.
24. Nashimoto,M. (1996) Specific cleavage of target RNAs from HIV-1 with 5′ half tRNA by mammalian tRNA 3′ processing endoribonuclease. *RNA*, **2**, 523–534.
25. Nashimoto,M., Geary,S., Tamura,M. and Kaspar,R. (1998) RNA heptamers that direct RNA cleavage by mammalian tRNA 3′ processing endoribonuclease. *Nucleic Acids Res.*, **26**, 2565–2571.
26. Nashimoto,M. (2000) Anomalous RNA substrates for mammalian tRNA 3′ processing endoribonuclease. *FEBS Lett.*, **472**, 179–186.
27. Takaku,H., Minagawa,A., Takagi,M. and Nashimoto,M. (2004) A novel four-base-recognizing RNA cutter that can remove the single 3′ terminal nucleotides from RNA molecules. *Nucleic Acids Res.*, **32**, e91.
28. Tamura,M., Nashimoto,C., Miyake,N., Daikuhara,Y., Ochi,K. and Nashimoto,M. (2003) Intracellular mRNA cleavage by 3′ tRNase under the direction of 2′-*O*-methyl RNA heptamers. *Nucleic Acids Res.*, **31**, 4354–4360.
29. Cormack,B.P., Valdivia,R.H. and Falkow,S. (1996) FACS-optimized mutants of the green fluorescent protein (GFP). *Gene*, **173**, 33–38.
30. Yang,T.T., Cheng,L. and Kain,S.R. (1996) Optimized codon usage and chromophore mutations provide enhanced sensitivity with the green fluorescent protein. *Nucleic Acids Res.*, **24**, 4592–4593.
31. Miller,A.D. and Rosman,G.J. (1989) Improved retroviral vectors for gene transfer. *BioTechniques*, **7**, 980–987.
32. Akkina,R.K., Walton,R.M., Chen,M.L., Li,Q.-X., Planelles,V. and Chen,I.Y. (1996) High-efficiency gene transfer into CD34+ cells with a human immunodeficiency virus type 1-based retroviral vector pseudotyped with vesicular stomatitis virus envelope glycoprotein G. *J. Virol.*, **70**, 2581–2585.
33. Landau,N.R. and Littman,D.R. (1992) Packaging system for rapid production of murine leukemia virus vectors with variable tropism. *J. Virol.*, **66**, 5110–5113.
34. Li,X., Mukai,T., Young,D., Frankel,S., Law,P. and Wong-Staal,F. (1998) Transduction of $CD34^+$ cells by a vesicular stomach virus protein G (VSV-G) pseudotyped HIV-1 vector. Stable gene expression in progeny cells, including dendritic cells. *J. Hum. Virol.*, **1**, 346–352.
35. Burns,J.C., Friedmann,T., Driever,W., Burrascano,M. and Yee,J.-K. (1993) Vesicular stomatitis virus G glycoprotein pseudotyped retroviral vectors: concentration to very high titer and efficient gene transfer into mammalian and non-mammalian cells. *Proc. Natl Acad. Sci. USA*, **90**, 8033–8037.
36. Yee,J.K., Miyanohara,A., Laforte,P., Bouic,K., Burns,J.C. and Friedman,T. (1994) A general method for the generation of high-titer, pantropic retroviral vectors: highly efficient infection of primary hepatocytes. *Proc. Natl Acad. Sci. USA*, **91**, 9564–9568.
37. Sakai,A., Hirabayasi,Y., Aizawa,S., Tanaka,M., Ida,S. and Oka,S. (1999) Investigation of a new p24 antigen detection system by the chemiluminescence-enzyme-immunoassay. *J. Jap. Assoc. Infect. Dis.*, **73**, 205–212.
38. Kuwasaki,T., Hosono,K., Takai,K., Ushijima,K., Nakashima,H., Saito,T., Yamamoto,N. and Takaku,H. (1996) Hairpin antisense oligonucleotides containing 2′-methoxynucleosides with base-pairing in the stem region at the 3′-end: penetration, localization, and anti-HIV activity. *Biochem. Biophys. Res. Commun.*, **228**, 623–631.
39. Clever,J., Mirandar,D.Jr and Parslow,T.G. (2002) RNA structure and packaging signals in the 5′ leader region of the human immunodeficiency virus type 1 genome. *J. Virol.*, **76**, 12381–12387.
40. McBride,M.S. and Panganiban,A.T. (1997) Position dependence of functional hairpins important for human immunodeficiency virus type 1 RNA encapsidation *in vivo*. *J. Virol.*, **71**, 2050–2058.
41. Sullenger,B.A., Gallardo,H.F., Ungers,G.E. and Gilboa,E. (1990) Overexpression of TAR sequences renders cells resistant to human immunodeficiency virus replication. *Cell*, **63**, 601–608.
42. Sullenger,B.A., Lee,T.C., Smith,C.A., Ungers,G.E. and Gilboa,E. (1990) Expression of chimeric tRNA-driven antisense transcripts renders NIH 3T3 cells highly resistant to Moloney murine leukemia virus replication. *Mol. Cell. Biol.*, **10**, 6512–6523.

43. Zhang,Y.A., Nemunaitis,J., Scanlon,K.J. and Tong,A.W. (2000) Anti-tumorigenic effect of K-ras ribozyme against human lung cancer cell line heterotransplants in nude mice. *Gene Ther.*, **7**, 2041–2050.
44. Habu,Y., Miyano-Kurosaki,N., Nagawa,T., Matsumoto,N., Takeuchi,H. and Takaku,H. (2002) Inhibition of HIV-1 replication by an HIV-1 dependent ribozyme expression vector with the Cre/loxP (ON/OFF) system. *Antivir. Chem. Chemother.*, **13**, 273–281.
45. Mulligan,R.C. (1993) The science of gene therapy. *Science*, **260**, 926–932.
46. Miller,A.D. and Rosman,G.J. (1989) Improved retroviral vectors for gene transfer. *BioTechniques*, **7**, 980–987.

Virus Genes (2006) 32:105–113
DOI 10.1007/s11262-005-5851-2

ORIGINAL ARTICLE

Analysis of human immunodeficiency virus type 1 integration by using a specific, sensitive and quantitative assay based on real-time polymerase chain reaction

Norio Yamamoto · Chika Tanaka · YuFeng Wu · Myint Oo Chang · Yoshio Inagaki · Yasunori Saito · Toshio Naito · Hitoshi Ogasawara · Iwao Sekigawa · Yasuo Hayashida

Received: 28 June 2005 / Accepted: 7 July 2005

Abstract A novel real-time nested-PCR assay was developed to quantify integrated human immunodeficiency virus type-1 (HIV-1) DNA with high specificity and sensitivity. This assay reproducibly allowed the detection of three copies of integrated HIV DNA in a background of 100,000 cell equivalents of human chromosomal DNA. The non-specific amplification of unintegrated HIV-1 DNA was significantly inhibited in this assay and the specificity of this assay was much higher than the previously reported method. This assay showed that kinetics in viral DNA sysnthesis was cell-type dependent and that the kinetics of HIV-1 DNA integration was very rapid in Jurkat T cell line. This method may provide new insights into the integration processes and be useful in evaluating future integrase inhibitors.

Keywords HIV-1 · Integration · *Alu*-PCR · Real-time PCR · Nested PCR

N. Yamamoto (✉) · YuFeng Wu · M. O. Chang · Y. Inagaki · Y. Saito
Department of Molecular Virology,
1-5-45 Yushima, 113-8519,
Bunkyo-ku, Tokyo, Japan
e-mail: norio.mmb@tmd.ac.jp

C. Tanaka · T. Naito · Y. Hayashida
Department of General Medicine,
Juntendo University School of Medicine,
2-1-1 Hongo, 113-8421,
Bunkyo-ku,
Tokyo, Japan

H. Ogasawara
Department of Internal Medicine and Rheumatology,
Juntendo University School of Medicine,
2-1-1 Hongo, 113-8421,
Bunkyo-ku,
Tokyo, Japan

I. Sekigawa
Institute for Environmental and Gender Specific Medicine,
Juntendo University Graduate School of Medicine,
2-1-1 Tomioka, 279-0021,
Urayasu-shi,
Chiba, Japan

Introduction

Integration of viral DNA into the host cell genome is common to all retroviruses and is indispensable for a productive human immunodeficiency virus type 1 (HIV-1) infection [1–4]. The RNA genome of HIV-1 is reversely transcribed into double-stranded linear DNA in the cytoplasm. The resulting linear DNA molecule is actively transported to the nucleus as a component of the preintegration complex, which is the immediate precursor for the integration reaction [5–9]. In addition, HIV-1 DNA circles with one or two long terminal repeats (LTRs) are also transported to the nucleus [10, 11].

In contrast to investigations on the unintegrated forms of HIV-1 DNA, quantitative analysis of integrated HIV DNA has been hampered by the lack of an appropriate assay. To distinguish between extrachromosomal and integrated HIV-1 DNA, several assays have been developed including *Alu*-HIV PCR, where a pair of primers anneal to the HIV-1 sequence and the highly repeated chromosomal *Alu* elements [12, 13]. However, previous *Alu*-HIV PCR methods have limited specificity due to the non-specific amplification of unintegrated HIV-1 DNA.

To accurately quantify integrated HIV-1 DNA with high specificity and sensitivity, we have developed a new method based on real-time nested *Alu*-HIV PCR. Using this method we analyzed viral DNA integration in several kinds of cells. In addition to the study of HIV-1 DNA integration, real-time PCR was used to monitor the copy number of total HIV-1 DNA and 2LTR circles during a single-round of viral replication.

Materials and methods

Cells, plasmids, and viruses

Peripheral blood mononuclear cells (PBMCs) were isolated with Ficoll-Paque PLUS (Amersham Biosciences AB, Uppsala, Sweden). Cells were washed twice with phosphate-buffered saline (PBS) and resuspended in RPMI 1640 with 10% fetal calf serum (FCS), 100 IU/ml of penicillin and 100 μg/ml of streptomycin. PBMCs were stimulated with 5 μg/ml of phytohemoagglutinin (PHA) and 100 U/ml of IL-2 or cultured without any stimulation. Jurkat cells, U937 cells and 293T cells were maintained in RPMI 1640 supplemented with 10% FCS and antibiotics.

The pNL-bsr delta env vector and the pNLE delta env vector were constructed by deleting the envelope-coding sequence of the NL4-3 genome and replacing a nef-coding sequence with a blasticidin resistance gene and EGFP gene, respectively. Virus stocks were prepared by cotransfection of 293T cells with a HIV-1-encoding plasmid and VSV-G expression vector.

Infection of cells with pseudotyped HIV-1

The virus stocks were treated with DNase-I to remove residual plasmid DNA. Cells were infected with VSV-G-pseudotyped NLE-delta env virus where the amount of p24 gag antigen was 30 ng per million cells. One hour after infection, the cells were washed three times with phosphate-buffered saline (PBS) and cultured in RPMI 1640 supplemented with 10% fetal calf serum. At each time point, one million cells were lysed with buffer for DNA extraction.

Generation of an integrated HIV-1 DNA standard

In order to precisely determine the copy number of integrated HIV-1 DNA, the standard cells should contain numerous randomized integration sites with a wide distribution of distances between the provirus and the nearest *Alu* sequences. To generate an appropriate HIV-1 DNA standard for quantification of integrated viral DNA, Jurkat cells were infected with NL-bsr delta env virus pseudotyped with VSV-G. Infected Jurkat cells were then cultured in the presence of blasticidin (10 μg/ml) to select cells which carried integrated viral DNA. Five days after initiation of the blasticidin selection, the number of resistant cells was counted. A total of one million cells were blasticidin-resistant, and the number of independent clones was estimated at more than 30,000. In our standard cell line, named Jurkat/NL-bsr, the copy number of integrated viral DNA is equal to the total HIV-1 DNA copy number because unintegrated forms of HIV-1 DNA were lost during the numerous rounds of cell division. Thus, based on total HIV-1 DNA and beta-globin quantifications, we estimated that, Jurkat/NL-bsr contained 5.44±0.05 proviruses per cell.

Real-time nested *Alu*-HIV PCR assay procedures

Real-time nested PCR was performed using an ABI-7700 sequence detector system (Applied Biosystems). During the first-round PCR, integrated HIV-1 sequences were amplified with the HIV-1 gag-specific primer (first-gag-R) and *Alu*-targeting primers (first-*Alu*-F and first-*Alu*-R) that annealed to conserved regions of the *Alu* repeat element (Fig. 1a). During the first-round PCR, *Alu*-gag sequences were amplified from 1/10 of total cell DNA in a 25 μl reaction mixture comprising 1×Taqman buffer A, 3.5 mM $MgCl_2$, 200 μM dNTP, 300 nM primers, 200 nM probe, and 0.025 U/μl AmpliTaq Gold. The first-round PCR cycle conditions were as follows: a DNA denaturation and polymerase activation step of 10 min at 95°C and then 12 cycles of amplification (95°C for 15 s, 60°C for 30 s, 72°C for 5 min). Due to the presence of numerous *Alu* elements within the human genome (at least 900,000 copies per haploid genome, giving an average distance of 4 kb between *Alu* elements [14]), abundant amplification of inter-*Alu* sequences occurred simultaneously with the amplification of *Alu*-HIV sequences. Only 12 cycles of amplification were performed to keep the reaction in the exponential phase.

During the second-round PCR, the first-round PCR product could be specifically amplified by using the tag-specific primer (second-tag-R) and the LTR primer (second-LTR-F) (Fig. 1b). The second-round PCR was performed on 1/25 of the first-round PCR product in a mixture comprising l× Taqman buffer A, 3.5 mM $MgCl_2$, 200 μM dNTP, 300 nM primers, 600 nM probe, and 0.025 U/μl AmpliTaq Gold. The second-round PCR cycles began with a DNA-denaturation and polymerase-activation step (95°C for 10 min), followed by 45 cycles of amplification (95°C for 15 s, 60°C for 60 s).

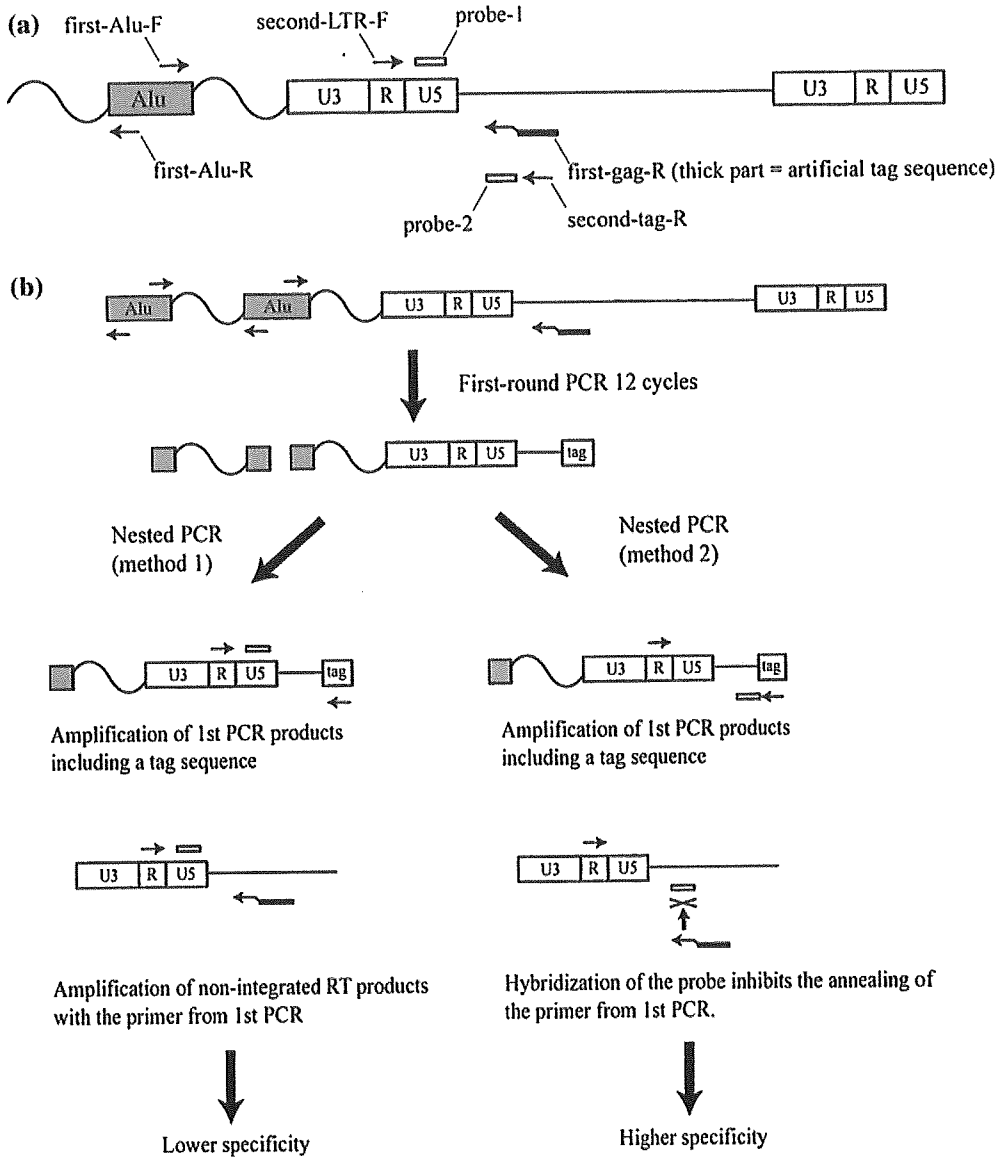

Fig. 1 Strategies for real-time nested PCR. (**a**) Location of primers and probes for the quantification of integrated HIV-1 DNA. (**b**) Comparison of two strategies to quantify integrated HIV-1 DNA

Real-time PCR assay for quantification of total viral DNA and 2LTR DNA

The total HIV-1 DNA copy number was determined with the primers that annealed in the U5 region of the LTR (total-F) and in the 5′ end of the gag gene (total-R) (Table 1). The 2LTR circles were amplified with primers spanning the LTR–LTR junction (circle-F and circle-R) (Table 1). The sequences of U5-gag and two-LTR junctions were amplified from 1/50 of total cell DNA according to the manufacturer's instructions. The copy numbers of total HIV-DNA and 2LTR circles were determined in reference to a standard curve prepared by amplification of quantities ranging from 10 to 100,000 copies of cloned DNA with matching sequences. The cell equivalents in sample DNA were calculated based on the amplification of the beta-globin gene (two copies per diploid cell) with ABI-7700 sequence detector system. The results of quantification were expressed as copy numbers per 1000 cells.

Results

Strategy of the previous real-time nested PCR and a novel real-time nested PCR

During the first-round PCR, integrated HIV-1 sequences were amplified with the HIV-1 gag-specific primer and

Table 1 Primer and probe sequences

Primer or probe	Sequence (5′-3′)	Target
first-*Alu*-F	AGCCTCCCGAGTAGCTGGGA	Integrated HIV-1 DNA (first-round PCR)
first-*Alu*-R	TTACAGGCATGAGCCACCG	
first-gag-R	CAATATCATACGCCGAGAGTGCGCGCTTCAGCAAG	
second-LTR-F	TTGTTACACCCTATGAGCCAGC	Integrated HIV-1 DNA (second-round PCR)
second-tag-R	CAATATCATACGCCGAGAGTGC	
probe-1	AGTGTGTGCCCGTCTGTTGTGTGACTC*	
probe-2	CGCTTCAGCAAGCCGAGTCCTGC*	
total-F	CCGTCTGTTGTGTGACTCTGG	Total HIV-1 DNA
total-R	GAGTCCTGCGTCGAGAGATCT	
total-probe	TCTAGCAGTGGCGCCCGAACAGG*	
circle-F	CCCTCAGACCCTTTTAGTCAGTG	2LTR circle DNA
circle-R	TGGTGTGTAGTTCTGCCAATCA	
circle-probe	TGTGGATCTACCACACACAAGGCTACTTCC*	

*Modified with FAM at the 5′ end and with TAMRA at the 3′ end. The tag sequence in the first-gag-R primer is underlined

Alu-targeting primers that annealed to conserved regions of the *Alu* repeat element (Fig. 1a). Since *Alu* elements are present in either orientation relative to the integrated provirus, the use of two outward-facing *Alu* primers optimized the amplification of *Alu*-gag sequences integrated into the host cell genome (Fig. 1a). To decrease amplification of nonintegrated reverse transcription products, we used an HIV-1 gag-specific primer extended with an artificial tag sequence at the 5′ end of the oligonucleotide (first-gag-R) in the first round of amplification and the primer which matches this artificial sequence (second-tag-R) in the second-round PCR (Fig. 1b).

The method 1 shown in Fig. 1b is equivalent to previously established real-time nested PCR assay and the method 2 is a novel assay developed by us. In the second-round PCR using the tag-specific primer and the LTR primer, the first-round PCR product could be amplified with lower background by the method 1. However, unintegrated viral DNA could be amplified in the method 1 even when the tag-specific primer was used for amplification. Because one twenty fifth of the reaction mixture after 12 cycles of the first-round PCR was used as a template for the second-round PCR, unintegrated reverse transcription products could be amplified with the forward primer for second-round PCR (second-LTR-F) and the residual reverse primer for first-round PCR (first-gag-R) (Fig. 1b). To prevent non-specific amplification of unintegrated reverse transcription products, we designed a new method (method 2) using probe-2 which has a sequence overlapping the first-gag-R primer. Probe-2 can preferentially hybridize to the target sequence and inhibit hybridization of the residual first-gag-R primer during the second-round PCR, because the melting temperature of probe-2 is much higher than that of the first-gag-R primer (Fig. 1b).

Specificity of the novel real-time nested PCR assay.

To assess the extent of non-specific amplification of unintegrated reverse transcription products in method 1 and method 2, we compared the fluorescence curves generated during the second-round PCR after three different first-round reactions: (1) in the presence of 3 primers (first-*alu*-F, first-*alu*-R, first-gag-R) with polymerase (primer+ / polymerase+), (2) in the presence of 3 primers without polymerase (primer+/polymerase−), and (3) in the absence of 3 primers without polymerase (primer−/ polymerase−). The fluorescence curve of primer+/polymerase+in the method 1 significantly shifted to the left in comparison to that of the primer−/polymerase−reaction (Fig. 2a). However, the fluorescence curve of primer+/polymerase−in the method 1 shifted as much as that of primer+/polymerase+ (Fig. 2a). This means that the extent of amplification of unintegrated reverse transcription products with the second-LTR-F primer and the first-gag-R primer was considerable. Probe-2, which was used in the method 2, preferentially hybridized to the target sequence and inhibited hybridization of the first-gag-R primer during the second-round PCR, because the melting temperature of probe-2 is much higher than that of the first-gag-R primer (Fig. 1b). As shown in Figure 2b, the fluorescence curve of primer+/ polymerase− in the method 2 shifted to the right dramatically compared with the curve of primer+/polymerise-in the method 1. The shift by using probe-2 instead of probe-1 was about 4 log10 units (17 cycles), which indicated that the specificity of the method 2 was much higher than that of the method 1.

Sensitivity of the novel real-time nested PCR assay.

The copy number of integrated HIV-1 DNA was determined in reference to a standard curve given by an array of serially

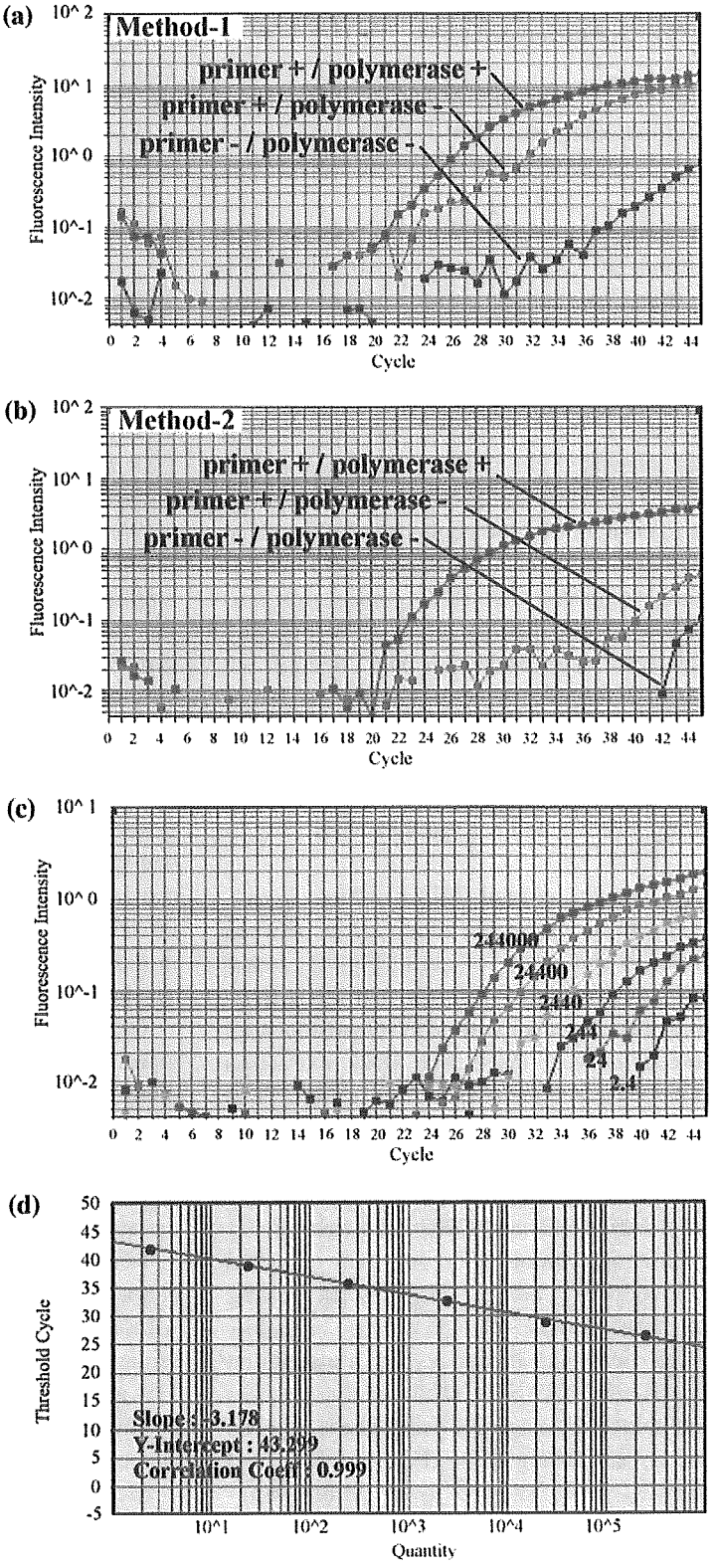

Fig. 2 Characteristics of real-time nested PCR. (**a** and **b**) Fluorescence curves generated by amplification of provirus DNA from HL60 cells infected with VSV-G-pseudotyped NLE delta env virus. (**a**) Fluorescence curves of probe-1 used in method 1. (**b**) Fluorescence Curves of probe-2 used in method 2. (**c**) Fluorescence curves generated by two-step amplification of serial dilutions of Jurkat/NL-bsr cell DNA. The copy numbers for each standard DNA are shown on the corresponding fluorescence curve. (**d**) Linear regression to quantify integrated HIV-1 DNA

diluted Jurkat/NL-bsr cell DNA mixed with uninfected Jurkat cell DNA to yield 100,000 cell equivalents. In our system, the regression obtained from amplification of serial dilutions of the integrated HIV-1 DNA was linear over a 6-log l0-unit range, and this *Alu*-HIV nested PCR allowed the detection of approximately three proviruses in 100,000 cell equivalents (Fig. 2c and 2d). The sensitivity of our system is as high as that of previously reported methods [15–18].

Analysis of early HIV-1 DNA synthesis in Jurkat cells infected with VSV-G-pseudotyped virus

To assess the time point when integration of HIV-1 takes place, we quantified integrated HIV-1 DNA in a single round of viral replication with the novel real-time nested PCR assay.

Total HIV-1 DNA was detected 3 h post infection and reached a maximum of 7,726 copies per 1000 cells at 5 h post infection (Fig. 3a). Subsequently a steep decrease phase and a slow decrease phase were observed. This novel real-time nested PCR assay detected integrated HIV-1 DNA within 3 h of infection, which indicated that reverse transcription products were imported to the nucleus immediately and integrated into the host cell genome very rapidly (Fig. 3b). The copy number of integrated proviruses reached a maximum of 1398 copies per 1000 cells at 5 h post infection and remained at the same level after this time point, which suggested that HIV-1 integration was completed by 5 h post infection in Jurkat cells (Fig. 3b). Two-LTR circles were detected by 3 h post infection but the copy number of 2LTR circles was not as high as that of integrated HIV-1 DNA. (Fig. 3c).

Comparison of viral DNA synthesis in Jurkat cells, U937 cells, resting PBMCs and activated PBMCs

We compared the kinetics of viral DNA synthesis in several kinds of cells to elucidate the relationship between viral DNA synthesis and status of cells (Fig. 4). Jurkat cells, U937 cells, unstimulated PBMCs and PHA/IL-2-activated PBMCs were infected with VSV-G pseudotyped HIV-1 and these cells were lysed with DNA extraction buffer at 3 h, 6 h, 12 h, 24 h and 48 h post infection. Time points of sample collection were determined based on the result of detailed kinetic analysis in Jurkat cells (Fig. 3).

Efficiency of reverse transcription was quite different in each type of cells. Jurkat cells and U937 cells were highly active in reverse transcription (Fig. 4a) and activated PBMCs were moderately active (Fig. 4b). In resting PBMCs reverse transcription efficiency was very low (Fig. 4b). Two cell lines with higher reverse transcription activity, Jurkat cells and U937 cells, exhibited three phases in the kinetics of total DNA: a rapid rising phase, a steep falling phase and a slow falling phase (Fig. 4a). Activated and resting PBMCs, which showed lower reverse transcription efficiency, exhibited only a slow rising phase (Fig. 4b).

The kinetics of viral DNA integration was also dependent on the cells. Integration of viral DNA in Jurkat cells and U937 cells was completed by 12 h post infection (Fig. 4c, d). Activated PBMCs showed complete integration in 24 h (Fig. 4d). The cope number of proviral DNA in resting PBMCs reached a maximum level at 48 h (Fig. 4d). Efficiency of 2LTR circle formation was different in each cell type. Synthesis of two LTR circles reached its peak at the same time point when viral DNA integration reached its maximum level (Fig. 4e, f). Ratio of 2LTR DNA to proviral DNA was low in all cells (0.1–0.6%)

Discussion

We could have developed a novel assay with high specificity and sensitivity to quantify integrated viral DNA of HIV-1. Our study showed that specificity of this nested PCR assay is much higher than that of the previously reported methods [15–19].

We could find four previous methods to quantify integrated viral DNA: (1) methods based on one-step amplification, (2) methods based on nested PCR using linker-primer (nested LP-PCR), (3) methods based on real-time nested PCR using *Alu*-specific primers and a virus-specific primer without tag sequence, (4) methods based on real-time nested PCR using *Alu*-specific primers and a virus-specific primer with tag sequence.

The novel real-time nested PCR assay detected integrated HIV-1 DNA as early as 3 h after infection while the one-step amplification method allowed the detection of proviral DNA later than 12 h [20] or 24 h [19] after infection. The delayed detection of integrated HIV-1 DNA in the one-step real-time PCR might be due to the limited sensitivity of this assay.

Other methods based on nested LP-PCR had been devised [15, 16]. The protocol of the nested LP-PCR involved many experimental steps, one of which is amplification of LTR in the second-round PCR. The nested LP-PCR amplified the LTR sequence and did not prevent the amplification of unintegrated forms of HIV-1 because of the absence of a tag sequence in the primer.

Recently, a real time nested PCR method with the *Alu* element-specific primers and HIV-1 gag-specific primer without tag sequence was described, in which the LTR sequence was amplified during the second-round PCR [17]. This real-time nested PCR did not prevent the amplification of unintegrated forms of HIV-1 due to the lack of tag sequence in the primer.

More recently, Brussel et al. [18] developed a new real-time nested PCR using an extended LTR primer with a tag sequence for the first-round PCR and the tag-specific primer for the second-round PCR to amplify only products from the first-round PCR. However, even this well-devised method could not prevent the residual tagged primer used in first-round PCR from annealing to the unintegrated forms of HIV-1 DNA, which resulted in lower specificity

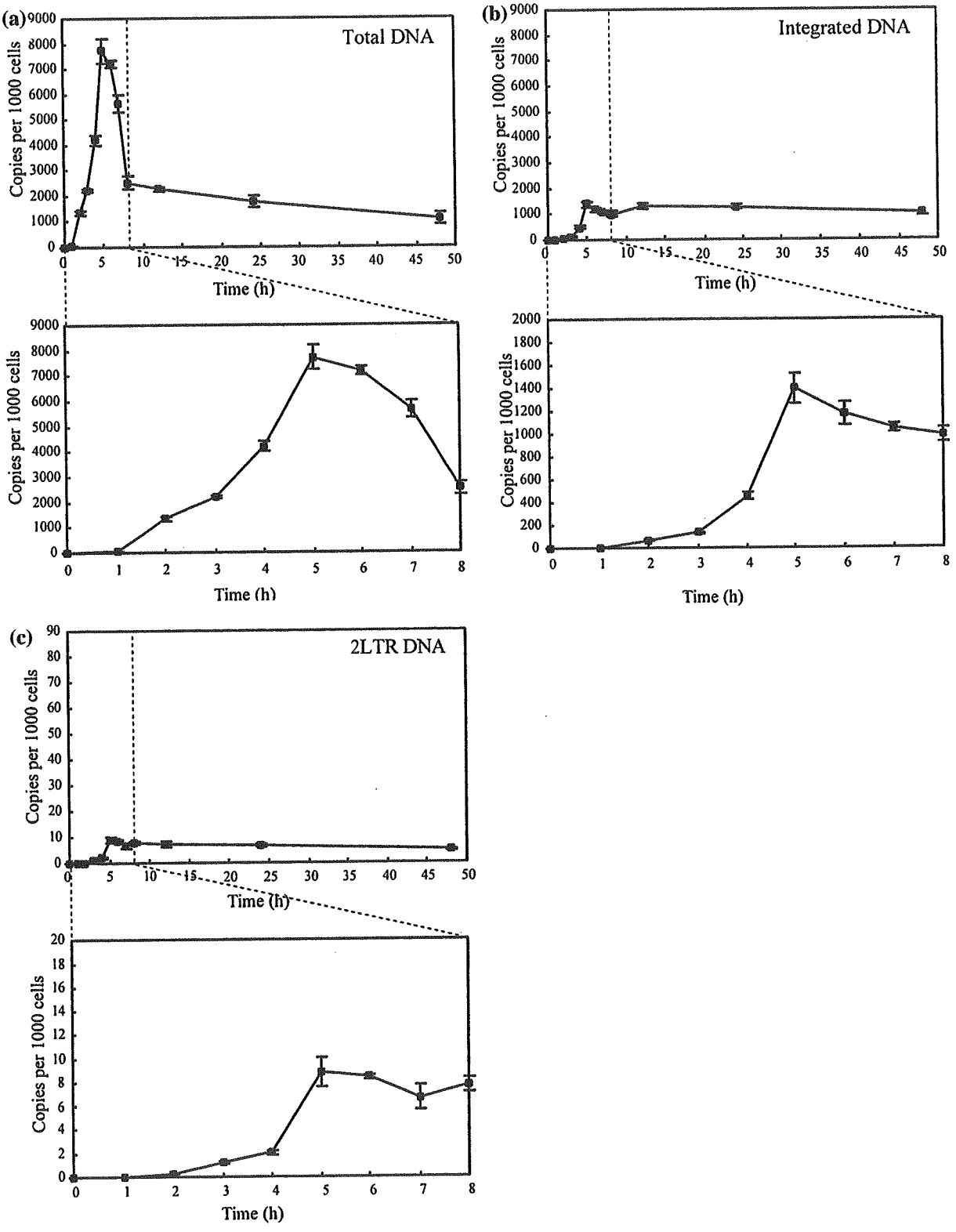

Fig. 3 Detailed quantification of HIV-1 DNA during a single round infection of Jurkat cells with VSV-G-pseudotyped NL-E delta env virus. (**a**) Time course analysis of total HIV-1 DNA, (**b**) integrated HIV-1 DNA and (**c**) 2LTR circle DNA. Values are shown as means±standard errors

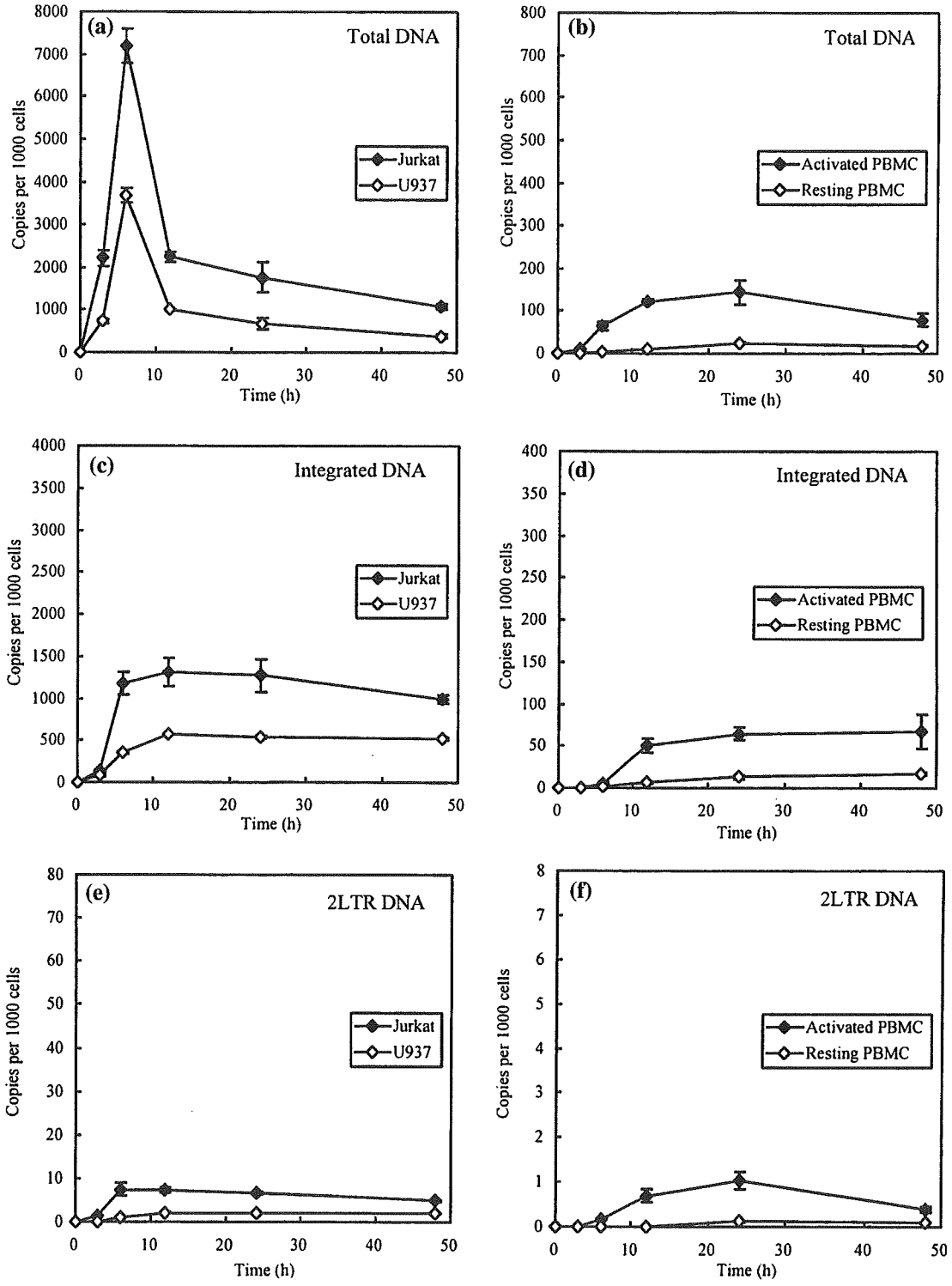

Fig. 4 Quantification of HIV-1 DNA synthesis during a single round infection of Jurkat cells, U937 cells, PHA/IL-2 activated PBMCs and resting PBMCs with VSV-G-pseudotyped NL-E delta env virus. (**a**) Time course analysis of total HIV-1 DNA synthesis in Jurkat cells and U937 cells, and (**b**) in PHA/IL-2 activated PBMCs and resting PBMCs. (**c**) Time course analysis of HIV-1 DNA integration in Jurkat cells and U937 cells, and (**d**) in PHA/IL-2 activated PBMCs and resting PBMCs. (**e**) Time course analysis of 2LTR DNA formation in Jurkat cells and U937 cells, and (**f**) in PHA/IL 2 activated PBMCs and resting PBMCs. Values are shown as means±standard errors

in the assay. The method 1 shown in Figs. 1 and 2 is equivalent to the real-time nested PCR developed by Brussel et al. and the method 2 is the new real-time nested PCR we have developed. Figs. 2a and b clearly demonstrated that specificity of our novel assay (method 2) was much higher than the previously reported method using a tag sequence. The probe-2 used in method 2 could inhibit the annealing of the residual tagged primer, which resulted in higher specificity than method 1.

By this novel assay, detailed kinetics of viral DNA synthesis was analyzed in Jurkat cells. Our assay detected integrated HIV-1 DNA within 3 h of infection, which emphasizes the sensitivity of this assay.

Then, we analyzed the kinetics of HIV-1 integration in U937 cells, activated PBMCs and resting PBMCs in addition to Jurkat cells. The kinetics of viral DNA integration depended on the cell type. HIV-1 DNA integration was completed 12 h after infection in Jurkat cells and U937 cells, 24 h in activated PBMCs and 48 h in resting PBMCs. Efficiency of viral integration was correlated with activity of reverse transcription. Jurkat cells exhibited the most rapid kinetics of reverse transcription and integration, and we may find the new factor(s) associated with reverse transcription and integration by investigating the molecules up-regulated or down-regulated in Jurkat cells.

The specific, sensitive and quantitative assay we have developed should prove useful in the kinetic studies of the integrated HIV-1 DNA especiallly during the early phase of infection. It should also prove applicable to clinical studies of viral integration and assessments of the effectiveness of future integrase inhibitors. Furthermore, it may be a valuable tool to test the integration efficiency of retroviral vectors designed for gene therapies.

Acknowledgements We thank Dr. Naoki Yamamoto for his support and helpful discussions. This work was supported by grants from the Ministry of Education, Science and Culture and the Ministry of Health, Labor and Welfare of Japan.

References

1. G. Englund, T.S. Theodore, E.O. Freed, A. Engleman, M.A. Martin, J. Virol. **69**, 3216–3219 (1995)
2. R.L. LaFemina, C.L. Schneider, H.L. Robbins, P.L. Callahan, K. LeGrow, E. Roth, W.A. Schleif, E.A. Emini, J. Virol. **66**, 7414–7419 (1992)
3. H. Sakai, M. Kawamura, J. Sakuragi, S. Sakuragi, R. Shibata, A. Ishimoto, N. Ono, S. Ueda, A. Adachi, J. Virol. **67**, 1169–1174 (1993)
4. M. Stevenson, T.L. Stanwick, M.P. Dempsey, C.A. Lamonica, EMBO J. **9**, 1551–1560 (1990)
5. M.I. Bukrinsky, N. Sharova, M.P. Dempsey, T.L. Stanwick, A.G. Bukrinskaya, S. Haggerty, M. Stevenson, Proc. Natl. Acad. Sci. USA **89**, 6580–6584 (1992)
6. M.I. Bukrinsky, N. Sharova, T.L. McDonald, T. Pushkarskaya, W.G. Tarpley, M. Stevenson, Proc. Natl. Acad. Sci. USA **90**, 6125–6129 (1993)
7. C.M. Farnet, F.D. Bushman, Cell **88**, 483–92 (1997)
8. L. Li, K. Yoder, M.S. Hansen, J. Olvera, M.D. Miller, F.D. Bushman, J. Virol. **74**, 10965–10974 (2000)
9. M.D. Miller, C.M. Farnet, F.D. Bushman, J. Virol. **71**, 5382–5390 (1997)
10. P. Barbosa, P. Charneau, N. Dumey, F. Clavel, AIDS Res. Hum. Retroviruses **10**, 53–59 (1994)
11. S.Y. Kim, R. Byrn, J. Groopman, D. Baltimore, J. Virol. **63**, 3708–3713 (1989)
12. T.W. Chun, L. Stuyver, S.B. Mizell, L.A. Ehler, J.A. Mican, M. Baseler, A.L. Lloyd, M.A. Nowak, A.S. Fauci, Proc. Natl. Acad. Sci. USA **94**, 13193–13197 (1997)
13. S. Sonza, A. Maerz, N. Deacon, J. Meanger, J. Mills, S. Crowe, J. Virol. **70**, 3863–3869 (1996)
14. R.J. Britten, W.F. Baron, D.B. Stout, E.H. Davidson, Proc. Natl. Acad. Sci. USA **85**, 4770–4774 (1988)
15. R. Kumar, N. Vandegraaff, L. Mundy, C.J. Burrell, P. Li, J. Virol. Methods **105**, 233–246 (2002)
16. N. Vandegraaff, R. Kumar, C.J. Burrell, P. Li, J. Virol. **75**, 11253–11260 (2001)
17. U. O'Doherty, W.J. Swiggard, D. Jeyakumar, D. McGain, M.H. Malim, J. Virol. **76**, 10942–10950 (2002)
18. A. Brussel, P. Sonigo, J. Virol. **77**, 10119–10124 (2003)
19. S.L. Butler, M.S. Hansen, F.D. Bushman, Natl. Med. **7**, 631–634 (2001)
20. S.L. Butler, E.P. Johnson, F.D. Bushman, J. Virol. **76**, 3739–3747 (2002)

HYBRIDOMA
Volume 24, Number 5, 2005

Production and Characterization of a Monoclonal Antibody Specific to Nef-Associated Factor 1 (Naf1)/A20-Binding Inhibitor of NF-κB Activation (ABIN-1)

MYINT OO CHANG,[1] NORIO YAMAMOTO,[1] SANKICHI HORIUCHI,[1] YU FENG WU,[1] MASAHIRO FUJIMOTO,[1] and NAOKI YAMAMOTO[1,2]

ABSTRACT

Cellular protein Naf1 (Nef-associated factor 1) or ABIN-1 (A20-binding inhibitor of NF-κB activation) is an important cellular protein, expressed in various human tissues and T-cell lines. Naf1 protein has two isoforms (Naf1α and Naf1β) with different C-termini, produced by alternative splicing. Naf1α and Naf1β have approximately 2800 and 2600 nucleotides, with an open reading frame of 1941 and 1781 nucleotides, encoding the 72-kDa Naf1α and 68-kDa Naf1β proteins, respectively. In the present study, we generated a monoclonal antibody (MAb) against human Naf1, which recognizes full-length, endogenous Naf1 of both isotypes. For this purpose, recombinant 6×His and myc-tagged N-terminal Naf1$^{38-135}$, Naf1(N) protein was produced by using the baculovirus expression system. Recombinant Naf1(N) protein was used to immunize Balb/c mice, and a hybridoma cell line producing stable and highly specific MAb with strong affinity to Naf1 was established. We further characterized this antibody by immunofluorescent assay and Western blot analysis to confirm effectiveness in detecting recombinant and endogenous Naf1. By Western blot analysis of recombinant Naf1-N fusion proteins with overlapping N-terminal sequences, the epitope targeted by anti-Naf1 MAb was determined as the 81–88–amino acid region of human Naf1.

INTRODUCTION

NAF1 (Nef-associated factor-1) or ABIN-1 (A20-binding inhibitor of NF-κB activation) is a cellular protein with four putative leucine zippers and four predicted regions of coiled coil structures. The gene encoding Naf1, which consists of 18 exons, is located on human chromosome 5q 32-33.1.[1] Naf1 mRNA is ubiquitously expressed in several human tissues, with strong expression in peripheral blood lymphocytes, spleen, and skeleton muscles. Naf1 is also detected in various human hematopoietic cell lines, such as Jurkat, Molt-4, H-9, and HL60.[1,2] According to the previous reports, Naf1 associates with human immunodeficiency virus type-1 (HIV-1) viral proteins Nef and matrix in the yeast two-hybrid system and pull-down assay using transfected human cell lysates.[1,2]

HIV-1 Nef not only enhances the viral infectivity, but also plays an important role in viral replication and pathogenesis.[3–10] Nef-defective HIV-1 virions are isolated from some cases of long-term non-progressors.[11] Nef induces down-regulation of cell surface expression levels of CD4 and major histocompatibility complex (MHC) class I molecules in HIV infection.[12–14] Thereby, Nef helps the virus to evade host defense and to increase viral infectivity.[15–17] CD4 is the primary receptor for HIV-1 and interferes with the infectivity of HIV-1 particles released from T cells.[18] Down-regulation of CD4 reduces the formation of complexes between CD4 and newly synthesized HIV-1 envelope protein on the infected cell surface, facilitating the release of HIV-1 virions. Nef-induced degradation of CD4 is also reported to result in the release of the normally CD4-bound tyrosine kinase, lck, and this could have a marked effect on signaling pathway in cellular activation. Because MHC class I is required to present viral peptide epitopes to cytotoxic T lymphocytes (CTL), down-regulation of cell surface MHC class I could inhibit the CTL-mediated lysis of HIV-

[1]Department of Molecular Virology, Bio-Response, Graduate School of Medicine, Tokyo Medical and Dental University, Tokyo, Japan.
[2]AIDS Research Center, National Institute of Infectious Diseases, Tokyo, Japan.

1–infected cells. Naf1 overexpression increases cell surface CD4 levels, but overexpression of Nef, in turn, inhibits Naf1-induced CD4 augmentation.[1]

Naf1 (ABIN-1) also interacts with A20 zinc finger protein in yeast two-hybrid screening. Zinc finger protein A20 has been characterized as a dual inhibitor of nuclear factor–kappa B (NF-κB) activation and tumor necrosis factor (TNF)–induced apoptosis.[19–24] NF-κB plays a pivotal role in immune and inflammatory responses through the regulation of the expression of several proteins, including pro-inflammatory cytokines, chemokines, and adhesion molecules. Uncontrolled activation of the NF-κB pathway is involved in the pathogenesis of several chronic inflammatory diseases and autoimmune diseases, such as rheumatoid arthritis, inflammatory bowel disease, and asthma. A20 binding protein Naf1 (ABIN-1) has been reported to inhibit NF-κB–dependent gene expression induced by TNF-α, and IL-1. Overexpression of Naf1 blocks NF-κB activation by TNF-α, and it is also thought that the expression of Naf1 is NF-κB dependent. It has been suggested that Naf1 takes a role in negative feedback regulation of NF-κB expression by competing with IKK-γ and also acts as an endogenous brake for the expression of some TNF-α–driven genes.[24–27] Moreover, Naf1 appeared to attenuate the EGF/ERK2 nuclear signaling, which is important for cell growth, differentiation, and cell death.[28] Nevertheless, intriguing questions regarding the mechanism of functions and regulation of Naf1 as well as the importance of physical associations between Naf1 and Naf1 interacting proteins, to carry out their functions in the molecular signaling pathways, remain to be answered.

For further understanding of the molecular mechanisms of the functions of Naf1, the most important tasks are to investigate intracellular localization, to investigate the relationship between the nucleocytoplasmic shuttling of Naf1 and its functions, and to discover Naf1-interacting proteins along with their functions. To perform these tasks, anti-Naf1 MAb is an essential tool, and in this report, we describe the production, characterization, and epitope mapping of an MAb specific to human cellular protein Naf1/ABIN-1. We also report the expression and subcellular localization of endogenous Naf1 in primary and various cell lines such as human PBL, Jurkat, MT-4, Molt-4, 293, and U-937 cell lines by using this MAb.

MATERIALS AND METHODS

Cell cultures

Spodoptera frugiperda (Sf9) cells were grown and maintained in complete Grace's insect medium (Gibco) supplemented with 10% fetal bovine serum (FBS), and *Trichoplusia ni* (High Five) cells in serum-free Sf-900II medium (Gibco). Both cell lines were cultured in monolayers at 27°C. SP2/0 murine myeloma cells, human PBL from a healthy adult donor, Jurkat, MT-4, Molt-4, 293, and U-937 cells were maintained in RPMI-1640 medium (Sigma) supplemented with 10% FBS, 100 U/mL of penicillin, and 100 μg/mL of streptomycin.

Construction of Naf1(N)-fusion protein cDNAs

cDNA encoding 6×His and myc-tagged Naf1(N) (amino acid residues 38–135) was constructed by polymerase chain re-

TABLE 1. OLIGONUCLEOTIDE PRIMERS USED FOR POLYMERASE CHAIN REACTION

Gene	*Primer*	*Sequences (5′ → 3′)*
Naf1(N)	His-Naf1(N)/F	CGCGGATCCGCGCATCATCATCATCATCATCAAGGGAT AAAGATGTTAGGGGAGC
	myc-Naf1(N)/R	CCGCTCGAGCGGCTAATTCAAGTCCTCTTCAGAAATG AGCTTTTGCTCCATTGAATTCTGCTCCTCAGGAGTGA
Naf1(N)-1	His-Naf1(N)-1/F	CGCGGATCCGCGCATCATCATCATCATCATATGCAAGG GATAAAGATGTTAGGG
	myc-Naf1(N)-1/R	CCCAGCTTGCTCTAATTCAAGTCCTCTTCAGAAATGA GCTTTTGCTCCAT CTCAGCCAGGGGGTCG
Naf1(N)-2	His-Naf1(N)-2/F	CGCGGATCCGCGCATCATCATCATCATCATGAGGAGCT AGTGAAGGACAACGA
	myc-Naf1(N)-2/R	CCCAAGCTTGCTCTAATTCAAGTCCTCTTCAGAAATGA GCTTTTGCTCCATGACTGGTGCTGGCTTGTCAC
Naf1(N)-3	His-Naf1(N)-3/F	CGCGGATCCGCGCATCATCATCATCATCATCTCACAGG AAAGGACTCAAATGTC
	His-Naf1(N)-3/R	CCCAAGCTTGCTCTAATTCAAGTCCTCTTCAGAAATGA GCTTTTGCTCCATTGAATTCTGCTCCTCAGGAGTG
Naf1(N)-A	His-Naf1(N)-A/F	CGCGGATCCGCGCATCATCATCATCATCAT GAGGAGCTAGTGAAGG ACAACGAGCTGCTCC
	myc-Naf1(N)-A/R	CCCAAGCTTCCATGGGCTCTAATTCAAGTCCTCTTCAG AAATGAGCTTTTGCTCCATAGGTGGTGGGAGCAGCT
Naf1(N)-B	His-Naf1(N)-B/F	CGCGGATCCGCGCATCATCATCATCATCATAACGAGCT GCTCCCACCACCTTCTCCCT
	myc-Naf1(N)-B/R	CCCAAGCTTCCATGGGCTCTAATTCAAGTCCTCTTCAG AAATGAGCTTTTGCTCCATGCCCAAGGAGGGAGAAG
Naf1(N)-C	His-Naf1(N)-C/F	CGCGGATCCGCGCATCATCATCATCATCAT
	myc-Naf1(N)-C/R	CCCAAGCTTCCATGGGCTCTAATTCAAGTCCTCTTCAG AAATGAGCTTTTGCTCCATCTCAGCCAGGGGGTCGA

action (PCR) technology, and the plasmid containing cDNA of full-length Naf1 was used as the template. The primers used in PCR reaction consisted of sense and antisense oligonucleotides containing *Bam*HI and *Xho*I sites respectively. The amplified cDNA was restricted by *Bam*HI/*Xho*I digestion, and subcloned into *Bam*HI/*Xho*I–digested pMelBacA baculovirus transfer vector (Invitrogen). cDNAs encoding 6 × His and myc-tagged Naf1(N) fusion protein fragments 1, 2, and 3, and A, B, and C were prepared by PCR amplification using specific primers with *Bam*HI and *Hind*III restriction sites, and ligated into pMAL-C2 vector containing MBP (maltose binding protein) sequence (Table 1). All constructs were confirmed by sequencing.

Generation of recombinant baculovirus in Sf9 cells

Recombinant baculovirus expressing Naf1(N) was produced by homologous recombination using Bac-N-Blue transfection kit (Invitrogen) according to procedures described previously.[29] Single viral clones were isolated by plaque assay and amplified by infecting Sf9 cells at a multiplicity of infection (MOI) of less than one. Infectivity was determined by titration and immunofluorescence staining of infected cells with mouse anti-myc MAb, followed by fluorescein isothiocyanate (FITC)–conjugated goat anti-mouse second antibody. Virus stock was stored in aliquots at −80°C.

Production of recombinant Naf1(N) protein in High Five cells

Exponentially growing High Five cells in 75-cm^2 tissue culture flasks were infected with the recombinant baculovirus at an MOI of 10–20 plaque-forming units (pfu)/cell and incubated at 27°C for 3–5 days. High Five cells were then sedimented by centrifugation, and supernatant was collected for purification using Ni-NTA columns (polyhistidine tag at the amino terminus of the recombinant Naf1(N) protein binds to Ni-NTA resin).[30–31] Purification of recombinant Naf1(N) protein was assessed by sodium dodecyl sulfate–polyacrylamide gel electrophoresis (SDS-PAGE) and silver staining.

Mice and immunization

Immunization, hybridoma preparation, and purification of MAb were done according to the procedures previously described.[32] In summary, three 6-week-old adult female Balb/c mice were immunized with three subcutaneous (s.c) injections of purified Naf1(N) protein at 2-week intervals. 100 μL of purified

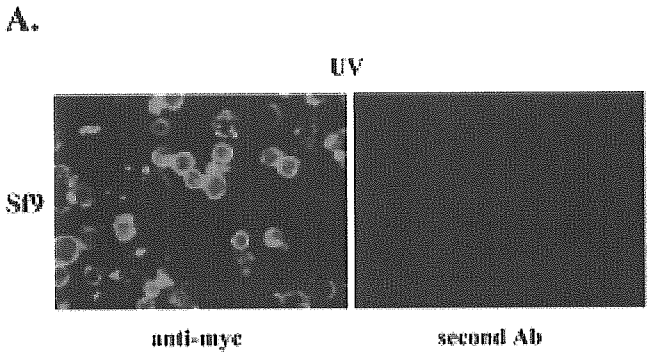

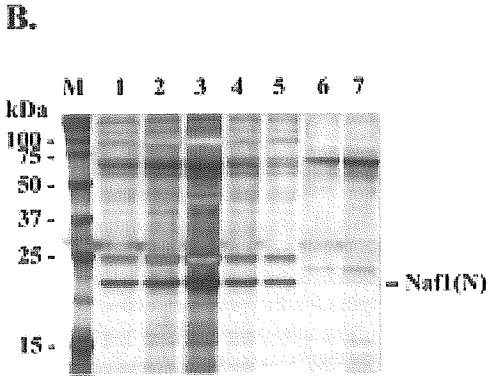

FIG. 1. (A) Immunofluorescence staining of Sf9 cells with anti-myc monoclonal antibody (MAb). Sf9 cells infected with baculovirus expressing 6×His and myc-tagged Naf1(N) were fixed in methanol and immunostained with anti-myc MAb, followed by fluorescein isothiocyanate (FITC)–conjugated second antibody (left panel) or with second antibody (Ab) only (right panel). (B) Sodium dodecyl sulfate–polyacrylamide gel electrophoresis (SDS-PAGE) and Silver staining of purified recombinant Naf1(N) protein. M, unstained precision plus protein marker; lane 1–5, elusion fraction E1 to E5; lane 6, wash; lane 7, flow-through. The arrowhead at the right indicates the purified target of Naf1(N) protein.